ASAR Wave Mode

- Description of Reprocessing Upgrade

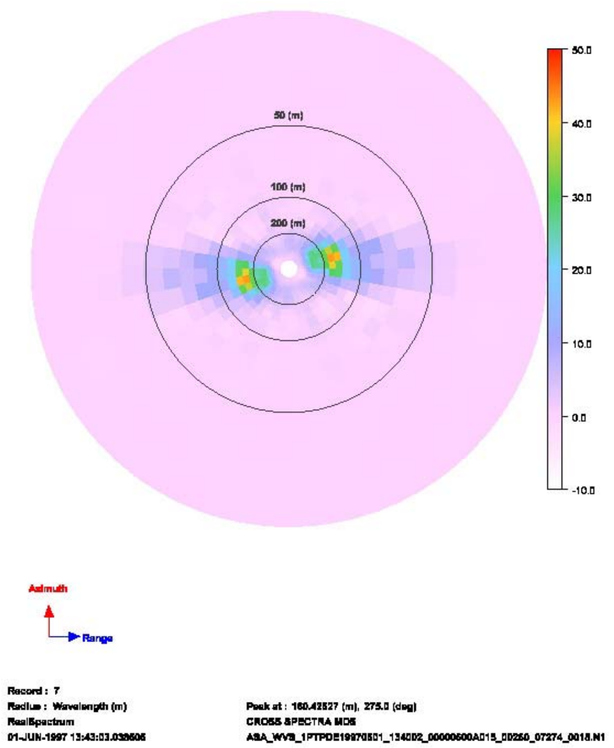

Document Title ASAR Wave Mode – description of reprocessing upgrade			
Author(s) Harald Johnsen , Fabrice Collard			
Contractor ESA/ESRIN		**Contracting Ref** 17376/03/I-OL	
ISSN 1503-1705 **ISBN 82-7747-128-9**	**Document No.** 3/2005	**Document Type** IT-Rapport	**Status/Availability** Open D7
Date 30th October 2005		**Version** 1.1	**No. of Pages** 22
Keywords Envisat ASAR Wave Mode, Wave Spectra, Calibration and Validation			
Notices			
Distribution ESA			
Reviewed by Kjell-Arild Høgda		**Technical Responsible** Jan-Børre Rydningen	

Abstract/Summary

Recommendations for upgrading the ASAR Wave Mode processing and products are presented in this report. This applies to the ASA_WVS_1B and the ASA_WVW_2B processing and products. The objectives of the upgrading are to improve the products as well as harmonizing the processing of the ASA_WVS_1B and the ASA_WVW_1B processing.

Appendix on the noise estimation is attached to the pdf file.

CONTENT

DOCUMENT CHANGE RECORD

Issue Rev. 0.9	all	Jun 2005
Issue Rev. 1.0	all	Aug 2005
Issue Rev. 1.1	all	Oct 2005

1 INTRODUCTION

The ASAR Wave Mode provides three products related to ocean wind and wave retrieval. These are the Level 1 Single-Look-Complex imagette, the Level1b cross-spectra, and the Level 2 SAR ocean wave spectra. The Level 1b cross-spectra product provides an estimate of the imagette cross-spectra, and is thus an engineering product. The Level 2 product provides estimates of the SAR ocean wave spectra and the local wind speed, and is thus a geophysical product. The objective of this report is to describe the necessary upgrade of the algorithms based on the validation that has been performed since the launch of the satellite. The proposed work will also include support during the reprocessing and validation activities. The upgrade of the WVS and WVW processing will also lead to a harmonization of the detrending and azimuth cut-off estimation procedures.

1.1 ACRONYMS

ASAR = Advanced Synthetic Aperture Radar
SUM = Software Users Manual
SRD = Software Requirements Document

2 REFERENCE AND APPLICABLE DOCUMENTS

2.1 APPLICABLE DOCUMENTS

[A-1] ENVI-CLCL-EOAD-SW-02-0027 Statement of work for technical support for global validation and long-term quality assessment of ASAR Wave mode products, Issue 1, 25 November 2002

[A-2] PO-SW-ESA-GS-00707 ENVISAT Ground Segment - ENVISAT ASAR Wind&Wave Measurements from Wave Mode Level 1b Product

[A-3] Johnsen H., Engen G., Lauknes I., The ENVISAT ASAR Wave Mode Cross Spectra Algorithm - Software Requirements Document, NORUT Report ASAR-D6-NT-01, v. 1.3.8, January 2004.

[A-4] Johnsen H., Engen G., Høgda K.A., B. Chapron,, ENVISAT ASAR Level 2 Wave Mode Product Algorithm Specification - Software Requirements Document, NORUT IT report IT650/1-01, v.2.2.7, August 2002.

[A-5] Johnsen H., Engen G., Lauknes I., The ENVISAT ASAR Wave Mode Cross Spectra Algorithm - Software User Manual and Installation Guide, NORUT Report ASAR-D16-NT-01, v. 1.3.2, January 2002.

[A-6] Johnsen H., Engen G., Høgda K.A., B. Chapron,, ENVISAT ASAR Level 2 Wave Mode Product Algorithm Specification - Software User Manual and Installation Guide, NORUT IT report IT650/3-01, v.1.2, December 2001.

2.2 REFERENCE DOCUMENTS

[B-1] PO-RS-ESA-GS-00245 ASAR Processing and Product Quality Requirements issue 3.

[B-2] Chapron B., Collard F., Johnsen H., Engen G., “ASAR Wave Mode First Geophysical Results”, Proc. of Envisat Calibration Review, SP-520 Proceedings, ISBN 92-9092-830-1, http://www.envisat.esa.int/.

[B-3] Johnsen H., Engen G., Chapron B., "Validation of ENVISATASAR Wave Mode Level 2 Product", Proc. of Envisat Calibration Review, SP-520 Proceedings, ISBN 92-9092-830-1, http://www.envisat.esa.int/.

[B-4] Johnsen H., Engen G., Chapron B., Walker N., Closa J., " Validation of ASAR Wave Mode Level 2 Product", Proc. of ENVISAT Cal/Val Workshop, ESA SP-531 Proceedings, http://www.envisat.esa.int/.

[B-5] Johnsen H., Kerbaol V., “Technical Support for Global Validation and Long-Term Quality Assessment and Optimization of ASAR Wave Mode Products: Specification of Parameters”, Norut IT/Boost Technologies Note, November 2003.

[B-6] Johnsen H., Kerbaol V., “Technical Support for Global Validation and Long-Term Quality Assessment and Optimization of ASAR Wave Mode Products: Cycle Reports”, Norut IT/Boost Technologies, Cycle Reports Nov03, Dec03, and Jan04.

[B-7] Kerbaol V., Johnsen H., Chapron B., Rosich B., “Quality assessment of ASAR Wave Mode products based on regional and seasonal comparison with WAM model outpust”, ERS/Envisat Symposium, 6-10 Sept. 2004, Salzburg

[B-8] Johnsen H., Engen G., Chapron B., “Validation of ASAR Wave Mode Level 2 product using WAM and buoy spectra”, Proceeding Coastal & Marine Applications of SAR, 8-12 Sept., 2003, Svalbard, ESA SP-565.

[B-9] Johnsen H., “Wind and Wave Data Calibration and Validation Results”, Norut IT Report IT750/2-2004 v1.1, January 2005.

[B-10] Mouche A., Hauser D., Kudryavtsev V., Daloze J-F., ”Multi-polarisation ocean radar cross-section from Envisat ASAR observations, ariborne polarimetric radar measurements and empirical or semi-emphirical models”, Proc. of 2004 Envisat & ERS Symposium, 6-10 Sept. 2004, Salzburg.

3 ALGORITHM UPGRADE

Based on the calibration and validation results [B-2], [B-3], [B-4], [B-5], [B-6], [B-7], [B-8], [B-9], the following upgrades of the ASAR Wave Mode WVS and the WVW products and algorithm are proposed.

3.1.1 WVS ALGORITHM UPGRADE

The main problems observed in this product that is related to the algorithm are:

a) inconsistency in the computation of image statistics

b) azimuth cut-off computation using the Newton iteration scheme

c) performance of the image detrending procedure – harmonization with the ASA_WVW procduct

a) Image Statistics

We propose to modify the computation so that the image statistics can be monitored in a Pearson Diagram. The following procedure can be used to compute the statistical parameters from the look extracted complex amplitude image of size $N_x \times N_y$ given by $A_{i,j}$:

$$\mu = \frac{1}{N_x N_y} \sum_{i=0}^{N_x-1} \sum_{j=0}^{N_y-1} \left| A_{i,j} \right|^2$$

$$\sigma^2 = \frac{1}{(N_x - 1)(N_y - 1)} \sum_{i=0}^{N_x-1} \sum_{j=0}^{N_y-1} \left(\left| A_{i,j} \right|^2 - \mu \right)^2$$

$$mean\_slc = \mu$$

$$\text{var}iance\_slc = \frac{\sigma^2}{\mu^2}$$

$$\beta_1 = squared\_skewness\_slc = \frac{\left(\frac{1}{N_x N_y} \sum_{i=0}^{N_x-1} \sum_{j=0}^{N_y-1} \left(\left| A_{i,j} \right|^2 - \mu \right)^3 \right)^2}{\left(\sigma^2 \right)^3}$$

$$\beta_2 = kurtosis\_slc = \frac{1}{N_x N_y} \frac{\sum_{i=0}^{N_x-1} \sum_{j=0}^{N_y-1} \left(\left| A_{i,j} \right|^2 - \mu \right)^4}{\left(\sigma^2 \right)^2}$$

The modification has been updated in the latest version (v1.3.8) of the software requirements document [A-3] and in the prototype software (v1.3.9). An upgraded version (v1.3.2) of the software user manual is also provided [A-5]. The documentations and the software are made available to ESA and to IFREMER for the reprocessing action.

b) Azimuth Cut-Off

The azimuth cut-off is at present computed by fitting the central part of the normalized azimuth profile, C_n , of the FFT^{-1} of the real part of the cross covariance spectra to a Gaussian roll-off function [A-3]:

$$\Delta F_{\lambda_c} = \sum_{n=n_{low}}^{n=n_{upp}} \left(C_n - e^{-\pi^2 (n-N_c)^2 \Delta y^2 / \lambda_c^2} \right)^2$$

with respect to the cut-off parameter, λ_c, using a Newton iteration scheme i.e. minimization of $\frac{\partial F_{\lambda_c}}{\partial \lambda_c} = 0$. Here $2N_c + 1$ is the number of pixels in the azimuth profile, Δy is the pixel spacing in the azimuth direction (given in meters), and n_{low}, n_{upp} are the lower and upper bounds (pixels) to do the fitting within. The Newton iteration scheme must be initiated with a first guess value for the cut-off, and shall then performs until max iterations are achieved or the RMS deviation is below certain predefined limit.

However, validation shows that the peak of the histogram of the azimuth cut-off values maximizes at the initial value (see Figure 1a) meaning that for large cases of data, no iteration is performed. The first guess value for the iteration is according to the set-up file equal to 200m, which corresponds to the peak value of the histogram in Figure 1. We have therefore implemented and tested another minimization approach that is more robust. This is called the Bisection Algorithm and is based on solving the equation:

$$\Delta f_{\lambda_c} = \sum_{n=n_{low}}^{n=n_{upp}} \left(C_n - e^{-\pi^2 (n-N_c)^2 \Delta y^2 / \lambda_c^2} \right) = 0$$

with λ_c on the interval $\left[\lambda_c^{min}, \lambda_c^{max}\right]$. Here $\Delta f_{\lambda_c = \lambda_c^{min}}$ and $\Delta f_{\lambda_c = \lambda_c^{max}}$ must have opposite sign.

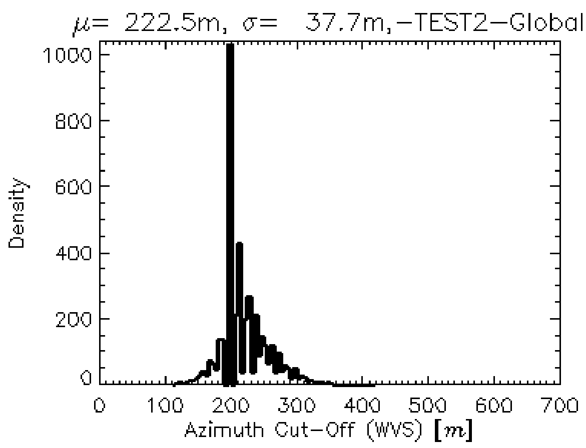

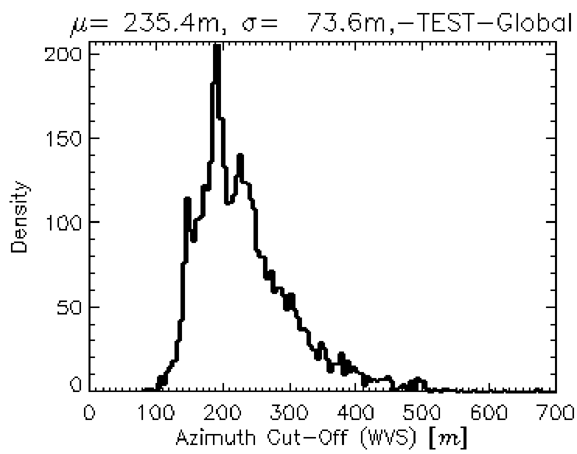

Figure 1 Left: Histogram of ASAR WVS azimuth cut-off parameter using the Newton iteration scheme. Right: Histogram of ASAR WVS azimuth cut-off parameter using the bisection algorithm described below.

Figure 1 shows that the Bisection algorithm performs much better than the Newton iteration scheme for this kind of minimization problem. The Bisection algorithm is well suited for cases where the function to be solved has opposite signs on the interval borders. This is typically in the case where fitting to a Gaussian function is required, as is the case here.
The bisection algorithm is implemented in the new version of the Level 1 prototype code.

c) Detrending

The removal of non-wave features is an important task, since it may corrupt the wave spectra retrieval at long wavelengths. This often happens in coastal areas. At present the detrending for the WVS product is performed by subtracting a tilted plane computed from average range and azimuth profiles [A-5]. However, for the WVW product the detrending is a little more advanced by dividing the SLC imagette by a low-pass filtered version of the same imagette [A-6]. The width of the low pass filter is specified in the set-up processing file. We will make the image domain detrending of the WVS product consistent with what is done for the WVW product. We thus propose to adapt the WVW procedure for the WVS product as well. The filter width will be specified in the processing set-up file and can easily be tailored to the image statistics such as the normalized image variance computed as described earlier, or other measures for the inhomogenity of the imagette.
In Figure 2 we demonstrate the impact of the low-pass detrending procedure on the imagette, by showing the imagette intensity before and after the detrending. A filter width of 300m is used for the detrending shown here, which corresponds to removing all wave components with wavelength larger than 600m.
The spatial detrending procedure is implemented in the new version of the Level 1 prototype code.

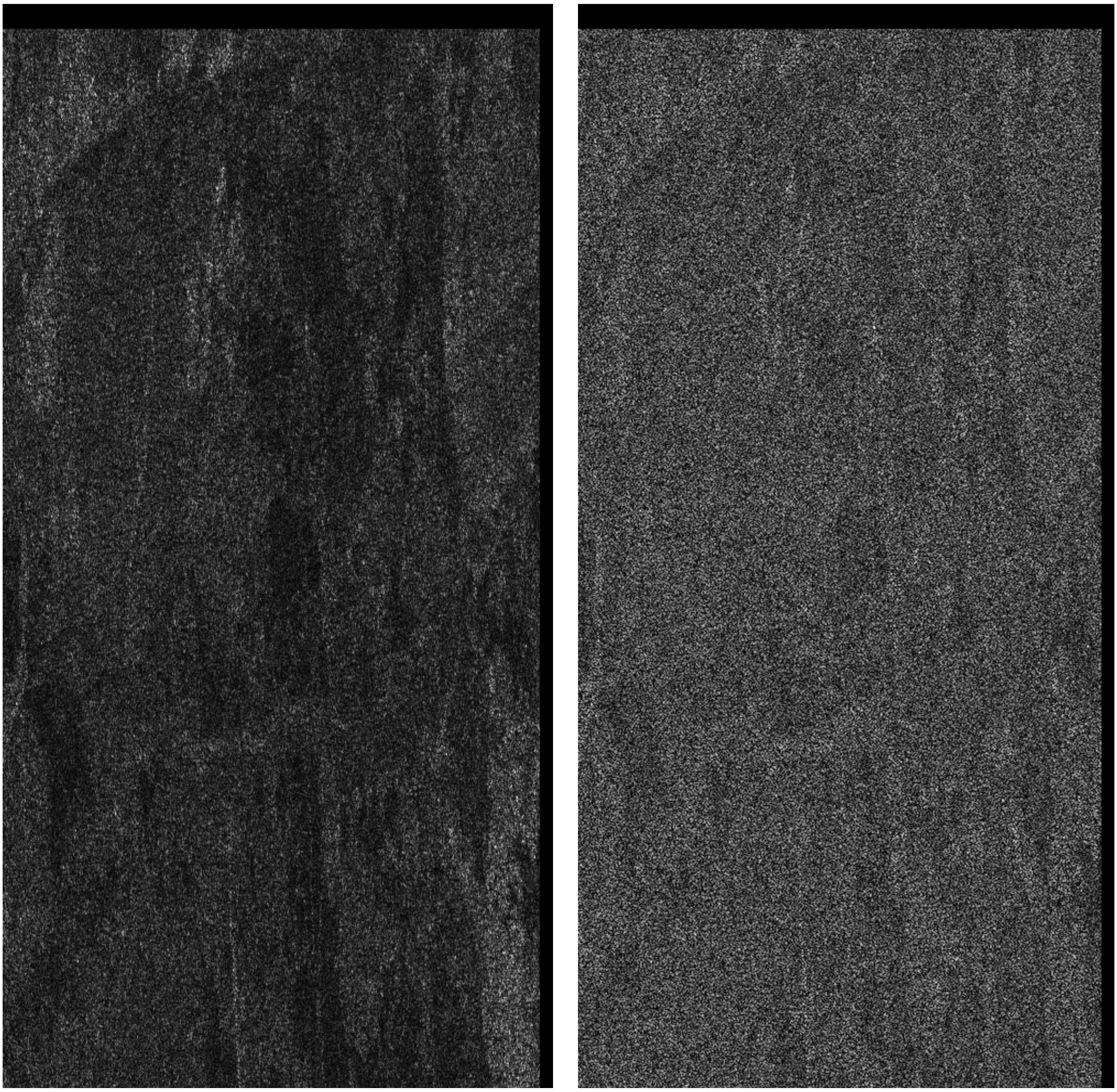

Figure 2 Example of ASAR WM imagette before (left) and after (right) detrending using the new lowpass based filtering of the SLC imagette. The filter width used in the right plot was 300m.

The impact of implementing the new detrending procedure on the ASA_WVS processing has been tested and the results are shown in the Figure 3. The results have been benchmarked against collocated WAM data. Here we show the histogram of the mean wave period difference between ASA_WVS cross-spectra and collocated WAM spectra, before and after the new detrending has been applied. A filter width of **300m** has been used in detrending the ASAR data.

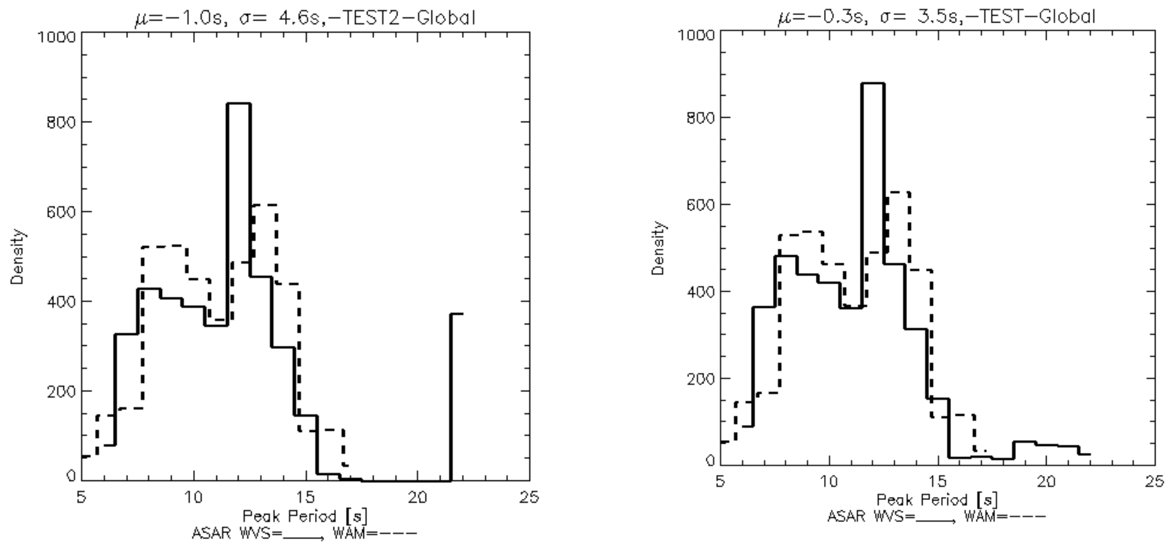

Figure 3 Histogram of difference between ASA_WVS cross-spectra peak period and ECMWF WAM peak period before (left) and after (right) applying the lowpass detrending procedure in the ASA_WVS processing. Filter width used is 300m.

Figure 3 shows that the lowpass detrending clearly improves the ASA_WVS peak period as compared to WAM. The large deviations observed at high periods (long wavelengths) are significantly reduced after the detrending, while the shorter periods are unchanged.

3.1.2 WVW ALGORITHM UPGRADE

The main problems observed related to the algorithm itself, and not to limitations in the instrument, are the following:

a) overestimation of significant waveheigth at low sea states, and lack of proper noise correction in the algorithm

b) limitations due to low resolution and dynamic range of look-up table, and only support for VV polarization.

c) azimuth cut-off – harmonization with the ASA_WVS product

d) estimation of non-linearity in the imaging process (i.e. wave age estimation)

e) interpretation of effects from slicks, current and other surface features as wave components

f) lack of information on the SAR wave spectra variance

g) improved ambiguity removal

h) improvement of transfer function at low frequencies

a) Significant waveheigth and noise correction

The first point is related to the use of CMOD-IF2 as the backscatter model in the look-up table [A-6]. The modulation transfer function (MTF) provided by the look-up table is also based upon the CMOD-IF2. We observe from Figure 4b) an inconsistency between observed and predicted radar cross-section at low wind speeds i.e. the ASAR measures lower backscatter values than predicted by CMOD-IF2. This will result in an underestimation of MTF at low wind speeds, and subsequently as an overestimation of waveheight at low wind speeds, as we observe in (Figure 4a).

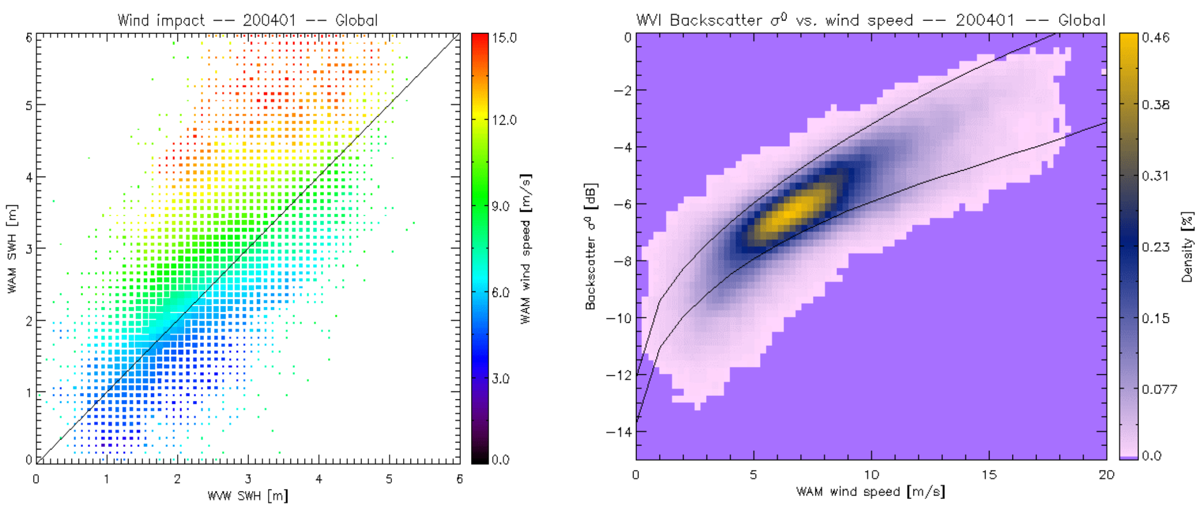

a) b)

Figure 4 a) Scatterplot of ASAR WVW significant waveheight versus ECMWF WAM significant waveheight color coded with wind speed. Bin size proportional to number of occurrences. b) ASAR WVW radar cross section versus wind speed over plotted the upper and lower limits as predicted by CMOD-IF2.

There are two issues that need to be investigated before we can solve this problem. These are:

1. We need to check if these deviations are a noise problem caused by the FBAQ 2 bit compression technique used in the ASAR Wave Mode data. If this is the case, the new version of the WVW code should be updated with a noise correction module. This means that we need to compensate the normalized radar cross section (NRSC) for the noise term.

2. If a noise correction is not needed, we will investigate whether or not the deviations between ASAR radar cross-section and CMOD-IF2 at low wind speeds are caused by errors in the co-located WAM wind speed. This can only be done when we have the WW3 product (i.e. ASA_WVW and WaveWatch along track co-located) available to compare with. If the WW3 shows similar deviations, a modification of the CMOD-IF2 to a SAR CMOD will be considered and the look-up table updated accordingly.

The noise estimation is coupled with the Doppler frequency estimation, and the method applies to both burst mode and standard mode data. Let I represent the true intensity image (as the instrument where imaging without bursts and with no additive noise) and let b be represent the envelope function representing burst modulation (equal to 1 or 0), and define the following function:

$$F(f,t) = I(t)b(t-\lambda f)a(\mu(f-f_c)),$$

where t represents the azimuth time and λ represents the time-frequency relation, and a is the azimuthal antenna pattern. Then the observed intensity in a burst mode data can be written as

$$\tilde{I}(t) = \int df\, F(f,t) + \sigma_N^2$$

and the azimuth Fourier profile as

$$\hat{I}(f) = \int dt\, F(f,t) + \sigma_N^2$$

where σ_N^2 is the variance of the additive noise. By combining the equations above the Fourier profile can be modeled by the following expression:

$$\hat{I}(f) = a(\mu(f-f_c))\int dt \frac{(\tilde{I}(t)-\sigma_N^2)b(t-\lambda f)}{\int df' b(t-\lambda f')a(\mu(f'-f_c))} + \sigma_N^2$$

where the two unknown are the Doppler frequency and the noise variance. We observe from the above equation that in the case of a conventional SAR (where b=1 form all pulses) that the equation is reduced to the normal model of a sum between a scaled version of the squared antenna diagram by the image intensity and the noise variance. In case of burst-mode data, the integral part will not generally be constant but modulates the azimuth Fourier-domain profile as function of the intensity distribution of the SAR data (known), the additive noise level (unknown), the length and location of the bursts (known) and the Doppler centroid frequency (unknown).

We have using the above approach, estimated and compared the noise component of the ASAR WM (WVI product) and the ASAR IM (IMS product) data. The noise is estimated from the azimuth Fourier profile of the complex images. The results are shown in Figure 5.

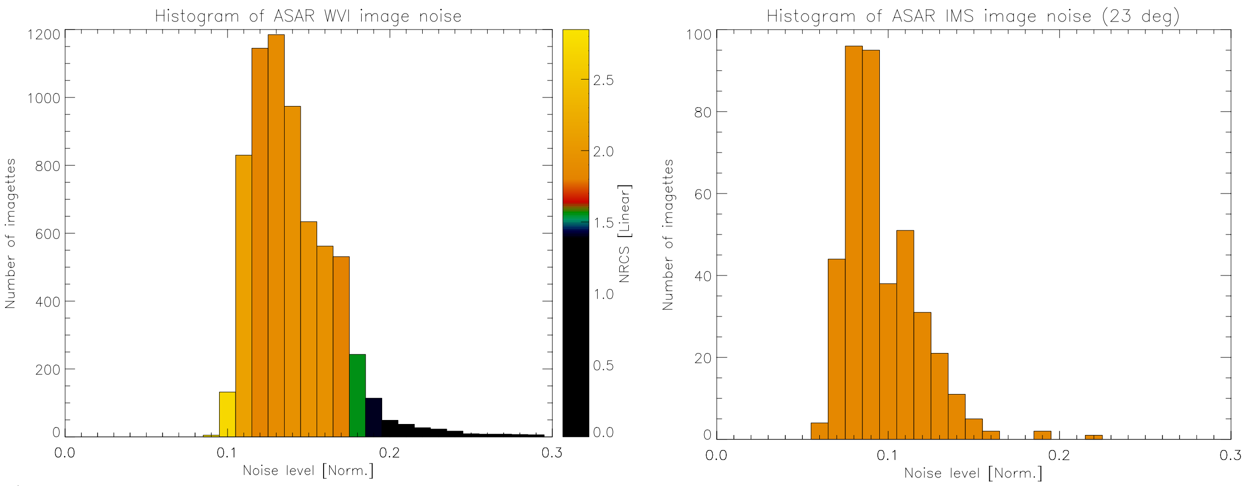

a) b)

Figure 5 Histogram of noise level estimated from ASAR Wave Mode a) and ASAR Image Mode b) complex images.

Figure 5 shows that the ASAR WVI imagettes have a higher noise level than the corresponding ASAR IMS imagette have. This is due to the FBAQ 2Bit compression applied to the WVI data. We also see the noise dependency of the NRSC. However, the data can easily be compensated for this by estimating the noise level for each imagette and compensating for the noise in the estimation of the NRSC. Since the cross-spectra used in the wave spectra retrieval is normalized with the NRSC, this correction will also impact the total energy of the ASA_WVW_2B wave spectra. The correction with respect to noise will also affect the MTF since the MTF is based on the radar cross-section and CMOD. **However, tests show that the impact of the noise correction on the significant waveheight is on average negligible**. **However, it might be of more importance when going to higher incidence angles for instance if the use the WM in S3 or S4 is considered**. **The noise correction is implemented in the new version of the prototype code.**

A short note on the approach to correct the WVW product with respect to noise term is attached to this document.

b) Look-up table - dynamic range , resolution, and HH polarization

The second point can easily be upgraded by increasing the sampling resolution and the dynamic range of the look-up table for the wind speed, wind direction, and wave age. ***Note that the software does not need to be modified when a new look-up table is added***. **The following range of values for the look-up table is generated for the new version of the prototype code**:

Parameters	**Start**	**Stop**	**Step**	**No of values**
Wind Speed (m/s)	0	26 (22)	1.5 (2)	22 (12)
WindDirection (deg)	0	90	22.5	5
Wave Age	0.42	2.0 (1.68)	0.13 (0.21)	13 (7)
Look-separation	0	0.447	0.2235	3

Table 1: Proposed upgrade of look-up table resolution and dynamic range. Numbers in parenthesis are current values. Wind direction and look-separation remain unchanged.

In addition the look-up tables for HH polarization will be proposed. The upgrade to hh polarization will be done by using the semi-empirical CMOD (or a modified SAR CMOD) in combination with a theoretically or semi-emphirical based closed form expression of the polarization ratio [B-8], [B-9], [B-10]. The use of the new models will capture the wind field variability of the polarization ratio. The models have been benchmarked against noise corrected ASAR AP mode data (Figure 6). This validation will continue with more in-situ collocated AP data.

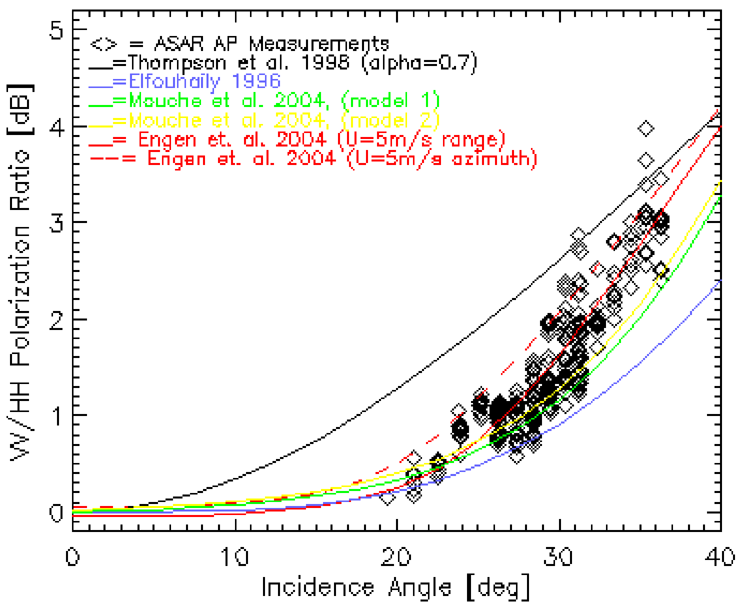

Figure 6 Polarization ratio ($^{vv}/_{hh}$) as function of incidence angle derived from ASAR Alt-Pol ocean images (◊), and the computed ratio from the GCM for range (solid) and azimuth (dashed) winds of 5 m/s. Polarization ratio from models in literature are plotted for comparison.

Look-up tables will be generated for both hh, vv polarization and incidence angles corresponding to swaths S1, S2, S3, and S4. **Semi-emphirical model based polarization ratios together with CMOD-IFR2 will be used to upgrade the look-up tables with HH polarization.**

c) Azimuth Cut-Off

For the WVW product the present azimuth cut-off value is computed from the estimated non-linear spectral width. This has shown to produce higher estimates of the cut-off wavelength than those obtained using the Gaussian roll-off function model (Figure 7). We propose to upgrade the cut-off estimation with the same procedure as proposed for the updated WVS processing as described in Chapter 3.1.1 b.

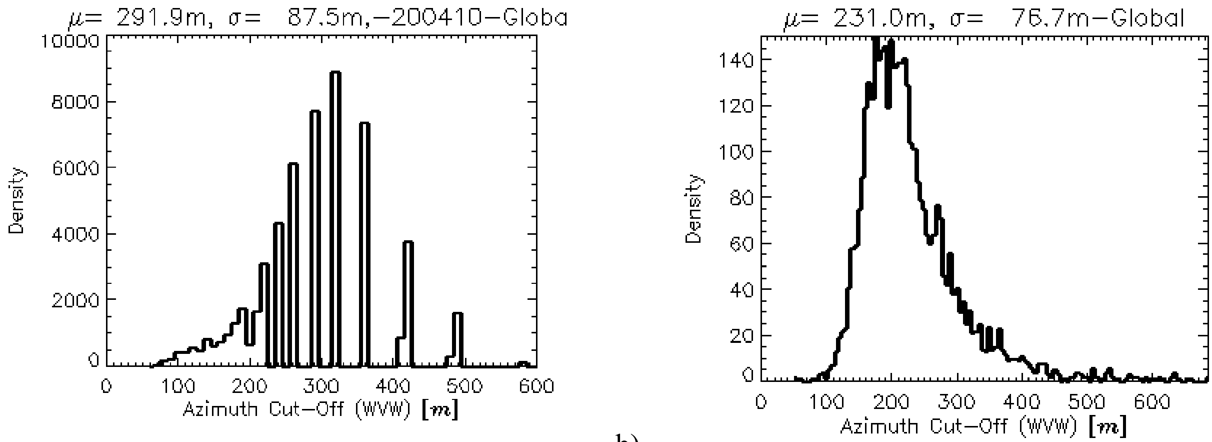

a) b)

Figure 7 Histogram of azimuth cut-off length from ASAR WM WVW. a) the old estimation procedure, b) the new estimation procedure.

The cut-off wavelength is used in the wave spectra retrieval as part of the total modulation transfer function, but also in defining the region of interest for the wave spectra retrieval. We have tested the impact of using the new approach on the estimate of the significant waveheight. This is shown in Figure 8, where we see that the new cut-off method slightly reduces the bias in the estimated significant waveheight. This can be understood since by using a higher cut-off value (as now) in the MTF, the waveheight will be overestimated.

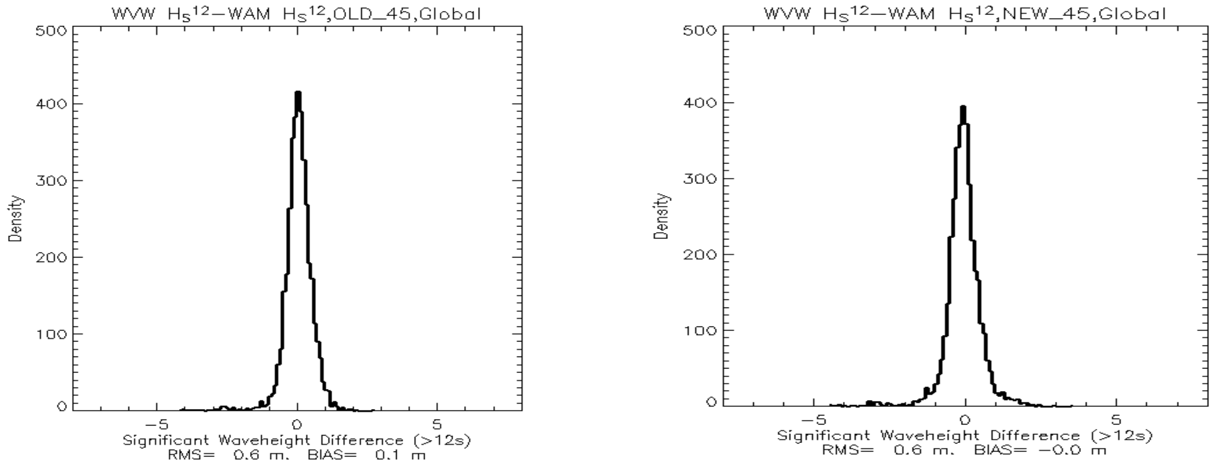

Figure 8 Histogram of swell significant waveheight difference between ASAR WVW and ECMWF WAM with the old (left) and the new (right) cut-off estimation procedure.

The new cut-off estimation procedure is implemented in the prototype code.

d) Estimation of non-linearity – wave age

The inversion scheme is a quasi-linear approach where the ASAR WM co- and cross-spectra are subtracted the non-linear part before the inversion is performed. The non-linear part is extracted from the look-up table using the wind field and wave age parameters. Thus we need to estimate the wave age and the wind field. The wind field is estimated combining the CMOD and the measured radar cross section, while the wave age is computed from the orbital velocity variance which again is directly assumed to be related to the non-linear spectral width. First we see that the operational code performs different from the prototype code (Figure 9). The prototype code seems to perform reasonably, although we have no data to validate the estimated wave age values. The operational code performs strange, with very discrete values. We have tested the prototype with the new look-up table (higher density and dynamic range of wave age), and some impact can be seen.

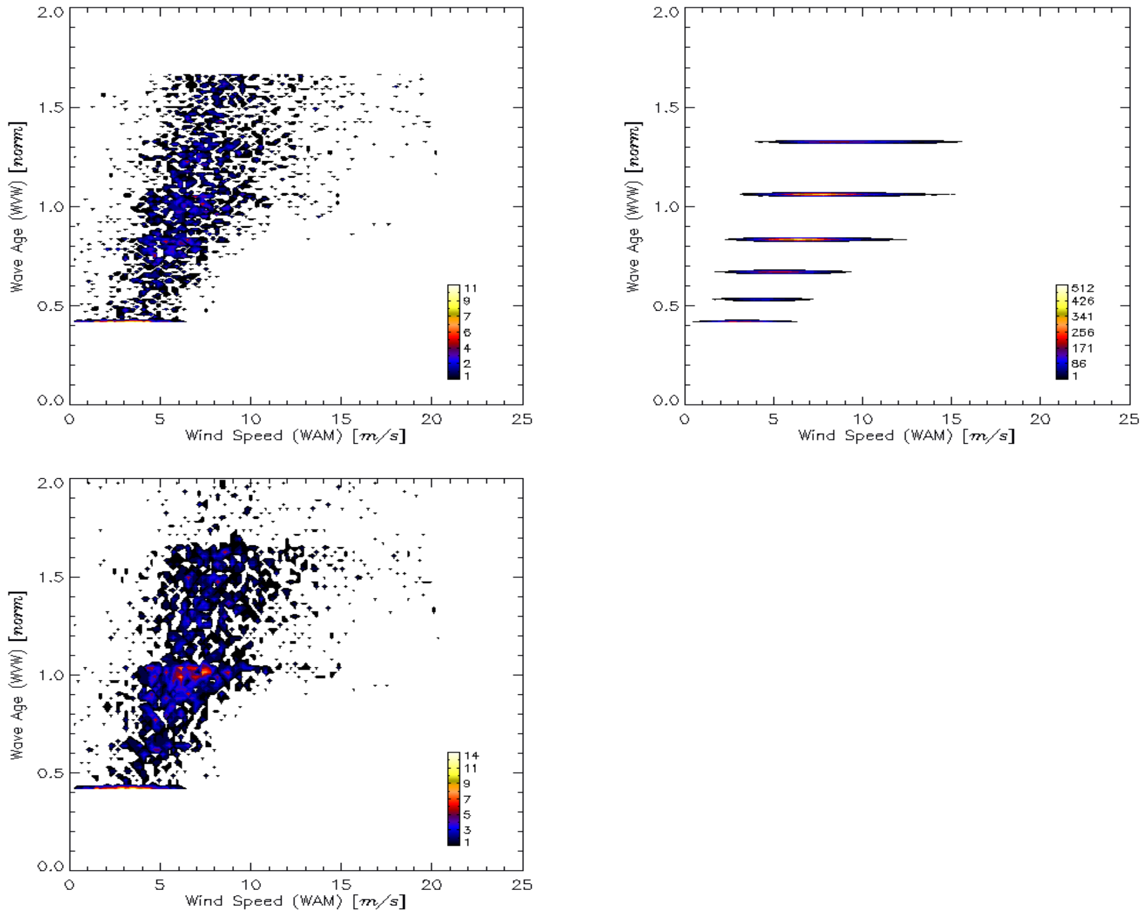

Figure 9 ASAR WVW wave age versus wind speed. Upper left plot is from the prototype products while the upper right plot is the ESA operational product. The lower left plot is the prototype with new look-up table (denser, and higher dynamic range).

Optionally, a new way of estimation the non-linear contribution will developed and tested (trying to minimize the contribution from swell). Instead of simply relating it to the inverse spectral width, we will estimate it as the wave age (given a wind field) where the non-linear energy exceeds the quasi-linear energy in the spectral domain. The challenge is to find the appropriate estimator. The look-up table will be used to develop the best estimator. **However, at present this is still a research task. Nevertheless, the problems with the current version of the PF-ASAR code must be solved in order to match the prototype output.**

e) Non-Wave features

For the WVW product, the detrending is performed by dividing the SLC imagette by a low-pass filtered version of the same imagette. The width of the low pass filter is specified in the set-up processing file. The problem here is to specify the optimal filter width for each imagette. We will use the same approach as the one proposed for the upgraded WVS processing (see Chapter 3.1.1 c). At present the WVW filter width is set to 500m meaning that features with wave lengths longer than 1000m are filtered out. Validation shows that we should decrease the filter width to 300m allowing only features with wave lengths longer than 600m.
An additional non wave feature removal is applied in the Fourrier domain by removing spectral contributions that are maximum at the cutoff frequencies (800m) and decreasing monotonically to higher wavenumbers. Example of result shown in Figure 10

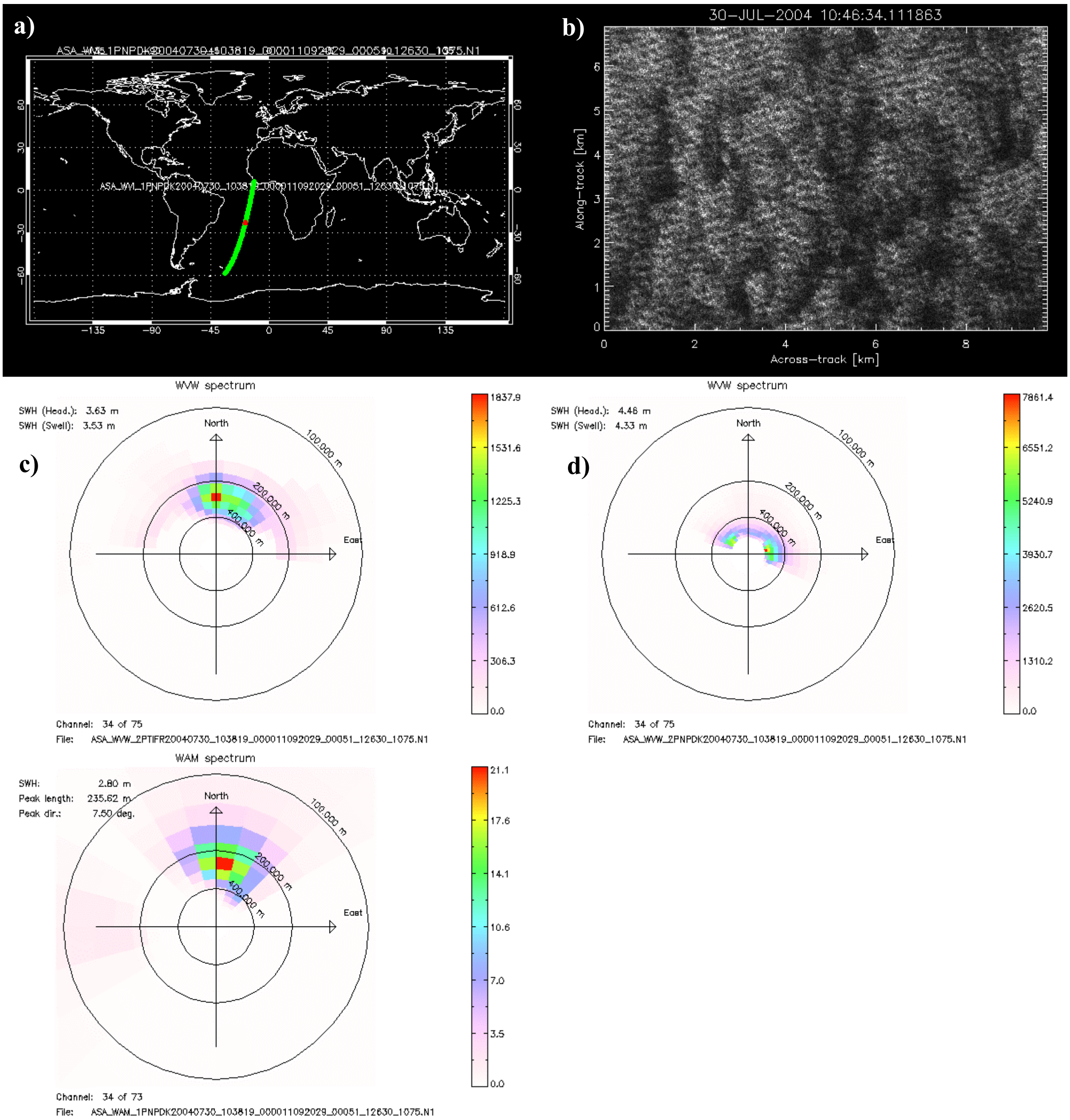

Figure 10 a) imagette location. b) imagette backscatter.c)Inverted wave spectrum (improved version) .d) Inverted wave spectrum (actual version). e) Collocated wave model spectrum

The adaptive low frequency filtering of the cross spectra is implemented in the prototype code.

f) SAR Wave spectra variance

At present there are no direct information in the ASA_WVW product about the wave spectra variances i.e. the uncertainty in each of the spectral components. This is important information for end-users in interpreting correctly the wave spectral information. We propose to estimate the variances at each spectral bins as part of the periodogram based cross-spectra estimation [A-4]. The number of periodograms (typically 23 pr imagette) is the ensemble to make the variance over. Let us denote $S^j(\underline{k})$ the periodogram of the *j*th subimage. The spectral variance for each wavenumber components of the cross spectra can then be computed as:

$$\overline{\mathrm{var}}\left(S^j(\underline{k})\right) = \frac{1}{N}\sum_{j=1}^{N}\left(S^j(\underline{k})\right)^2 - \left\langle S(\underline{k})\right\rangle^2$$

where $\langle\ \rangle$ denotes the standard mean value estimator, and N is the number of periodograms. The corresponding wave spectra variances are then computed using the same approach used for computing the wave spectra from the cross spectra. **However, the inclusion of the wave spectral variances, requires modification of the output product format**. **The variance estimate is not implemented in the prototype code**. In Figure 11 example of variance spectra is shown.

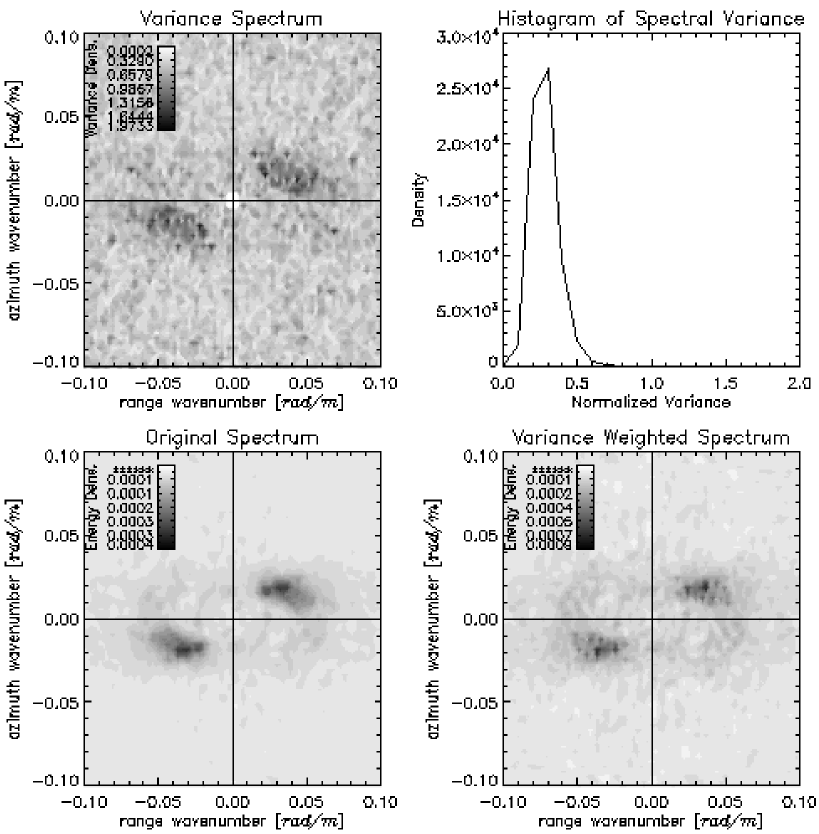

Figure 11 Upper left: Variance spectra computed over the 42 periodograms. Upper right: Histogram of spectral variance. Lower left: Real part of cross-spectra. Lower right: Real part of cross-spectra weighted with variance spectra.

g) Improved ambiguity removal

Ambiguity removal is based generating a symmetric and a anti-symmetric wave spectra by applying the modulation transfer function (MTF) on the real and imaginary parts of the cross-spectra, respectively. Then only those wave component in the symmetric spectrum with values above certain positive value in the anti-symmetric spectra are kept. However, it has turned out that the imaginary part of the cross-spectra has often a low SNR, which in combination with the MTF may produce ambiguities in the wave direction retrievals. We thus recommend to apply on the imaginary part of the cross-spectra a modified MTF that is thresholded to avoid noise amplification at low frequencies and a weighting function based on the ambiguous inverted wave spectrum.

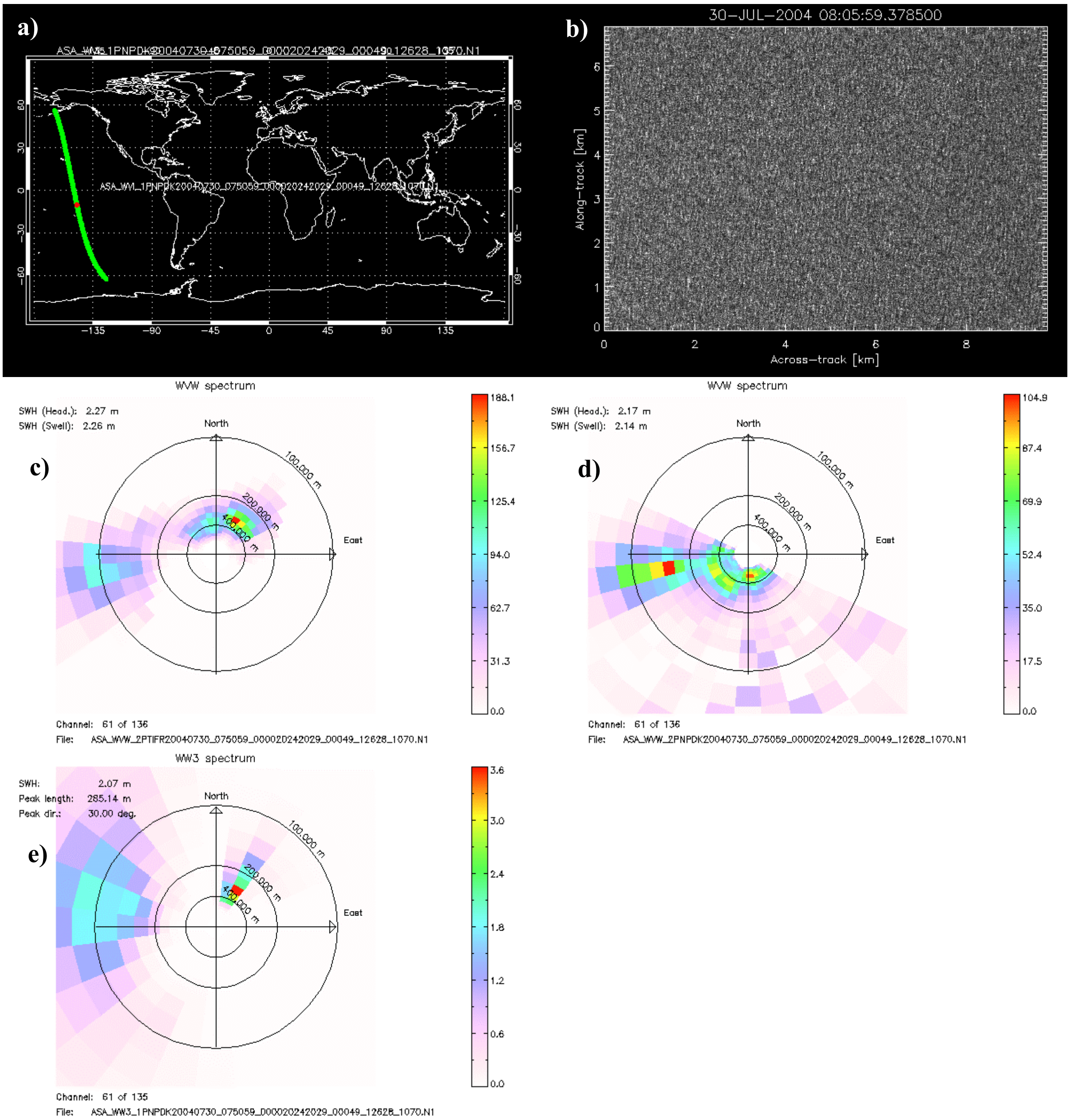

Figure 12 : a) imagette location. b) imagette backscatter.c)Inverted wave spectrum (improved version) .d) Inverted wave spectrum (actual version). e) Collocated wave model spectrum

This improvement in ambiguity removal has a strong impact when several wave systems are present at the ocean surface since the imaginary part of the longer wave system might have an SNR lower than the some surrounding low frequencies or noise contribution. Figure 12 illustrates a swell system in the tropical part of the Pacific ocean that has been located in the wind sea direction whereas the improved ambiguity removal allows this swell system to have an independent propagation direction towards the North East.

Additionally a new parameter (*ambiFac* instead of *signal-to-noise*) is used to assess the confidence flag of the swell inversion. The *ambiFac* is also stored in the spare field of the *OCEAN WAVE SPECTRA MDS*.

The improved ambiguity removal is implemented in the prototype code, and an improved confidence measure is implemented.

h) Improvement of transfer function at low frequencies

It has been observed that the actual SAR MTF tends to overestimate the swell at low wavenumbers. This has the double impact of reducing the relative importance of rather developed wind seas (in the range 100-200m) and overestimating the wavelength of swell systems. This artefact is due to the assumption that all spectral components of the wave spectrum are free propagating waves. This assumption is no longer valid for wavenumber lower than the spectral peak which are not propagating waves but effects of wave groupiness (limited number of waves within a group equivalent to a peak broadening in the spectral domain). We thus suggest to apply on wavenumber lower than the peak for each single direction the same transfer function as for the peak wavenumber.

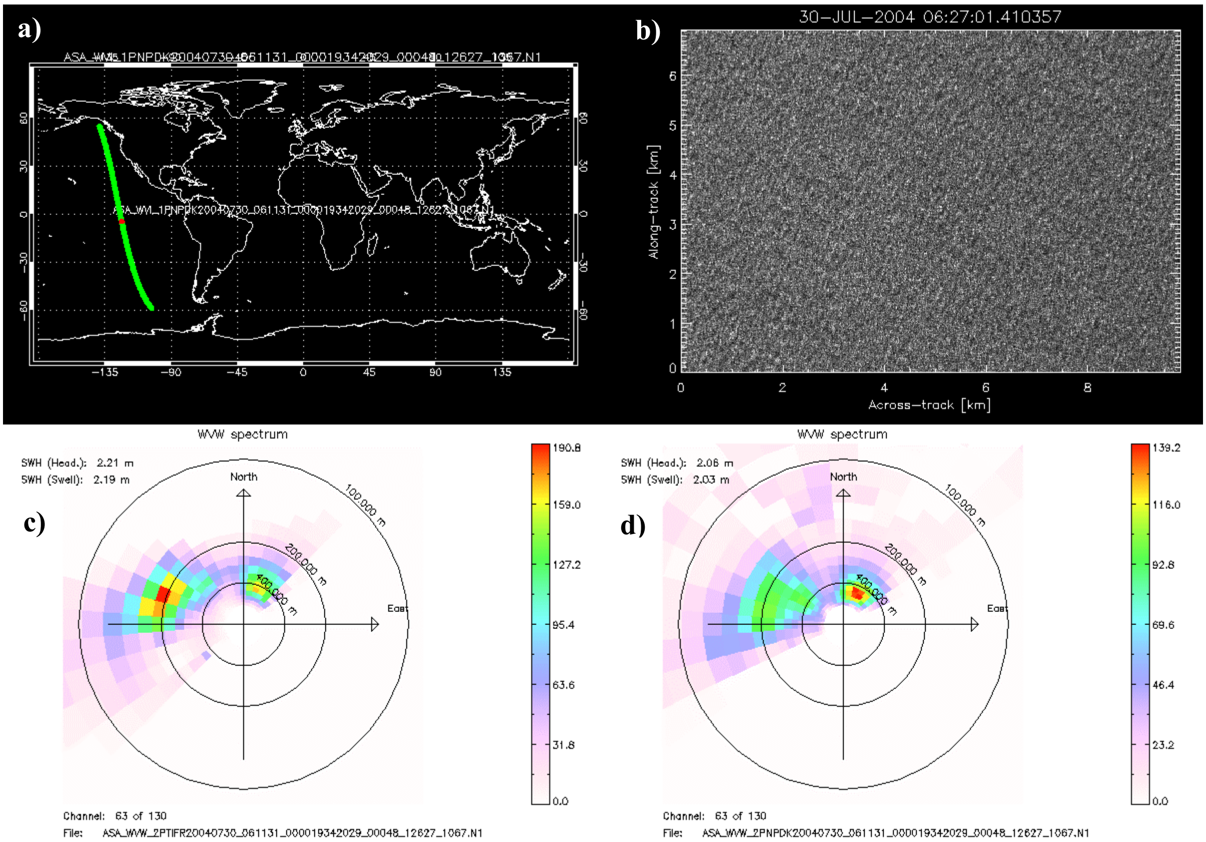

e)

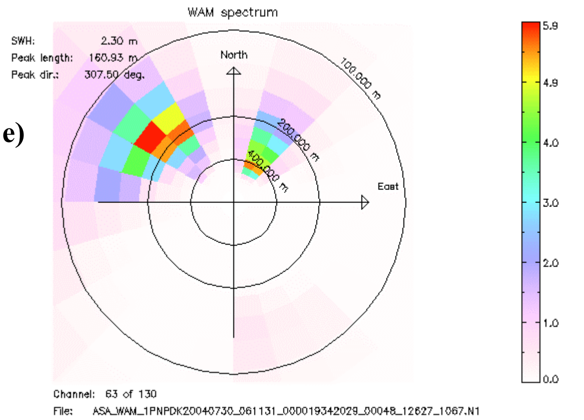

Figure 13 a) imagette location. b) imagette backscatter.c)Inverted wave spectrum (actual version) .d) Inverted wave spectrum (improved version). e) Collocated wave model spectrum

From the analysis of the actual inverted wave spectrum, one can believe that the retrieved spectrum is limited to long waves. As illustrated in Figure 13, it appears that, when correcting for the overestimation of the MTF at low wavenumber, the retrieved wave spectra have a large information content in the wind sea part (100-200m) that is comparable to that of 3rd generation numerical wave models (WAM/WW3).

The improvement of transfer function at low frequencies is implemented in the prototype code.

4 SUMMARY TABLE

Product ID	Description of upgrade	Implementation Status	Documentation Status	Testing Status	Validation Status
ASA_WVS_1B	inconsistency in the computation of image statistics	OK	OK	OK	Open
	azimuth cut-off computation using the bisection algorithm instead of Newton iteration scheme	OK	OK	OK	Open
	performance of the image detrending procedure – harmonization with the ASA_WVW procduct	OK	OK	OK	Open
ASA_WVW_2B	overestimation of significant waveheigth at low sea states, - noise correction , - calibration & MTF	OK	OK	OK	Open
	limitations due to low resolution and dynamic range of look-up table, and only support for VV polarization.	OK[1]	OK	Open (not tested on HH data)	Open
	azimuth cut-off – harmonization with the ASA_WVS product	OK	OK	OK	Open
	estimation of non-linearity in the imaging process (i.e. new wave age estimation procedure)	Not considered[2]			
	interpretation of effects from slicks, current and other surface features as wave components	OK	OK	OK	Open
	lack of information on the SAR wave spectra variance	Not considered			
	improved ambiguity removal	OK	OK	OK	Open
	improved low wavenumber MTF	OK	OK	OK	Open

[1] Look-up tables modified , but at present no support for HH polarization
[2] However, the current PF-ASAR version must be updated to match the prototype version

Note on estimation of noise in ASAR WM-data

Geir Engen

June 18, 2005

Background Theory

The basic idea behind the estimation of additative noise is that the noise is is not colored by the antenna pattern while the coherent signal from a ground target is. The additative noise w_{noise} can be written as a sum of two contributions; AD-noise (also containing the termal noise) and compression noise:

$$w_{\text{noise}} \;=\; w_{\text{ad}} + w_{\text{comp}} \tag{1}$$

Let I_{c} represents the complex SAR data, then the (azimuth direction) profile of the Fourier domain of can be written as

$$b(f) \;\equiv\; \mathrm{E}\{|\hat{I}_{\text{c}}(f)|^2\} \;=\; I\,\tilde{a}^2(f - f_{\text{cd}}) + \tfrac{1}{F}\,\sigma^2_{\text{noise}} \tag{2}$$

where $\hat{I}_{\text{c}}$ is the Fourier transform of the complex SAR data, I is the average intensity of the coherent signal, σ^2_{noise} is the variance of the additative noise term w_{noise}, f is the azimuth direction frequency and F is the frequency support length (bandwidth). The antenna profile $\tilde{a}$ is shifted by the dopppler frequency f_{dc} and normalized to have integral value equal to one. by comparing this model width the observed azimuth Fourier profile the three unknown; I, σ^2_{noise} and f_{dc} can be estimated.

The observed intensity of the SAR data is given by

$$\tilde{I} \;=\; \int_{-F/2}^{F/2} df\, b(f) \;=\; I + \sigma^2_{\text{noise}}\,. \tag{3}$$

A reasonable model for the compression part of the noise variance is tho assume it is proportional to the output signal level of the AD-converter, we have the following model for the noise variance:

$$\sigma^2_{\text{noise}} \;=\; \sigma^2_{\text{ad}} + \alpha\,(I + \sigma^2_{\text{ad}})\,. \tag{4}$$

In Figure 1 is the noise fraction of the total intensity $\sigma^2_{\text{noise}}/(I + \sigma^2_{\text{noise}})$ plotet as function of signal intensity I. The data-set shown, represents the total recording of May 2004 (26,930 imagettes). The solid line represents the theoretical line according to the noise model of equation (4), with $\alpha = 0.069$ and $\sigma^2_{\text{dc}} = 7.5 \cdot 10^2$.

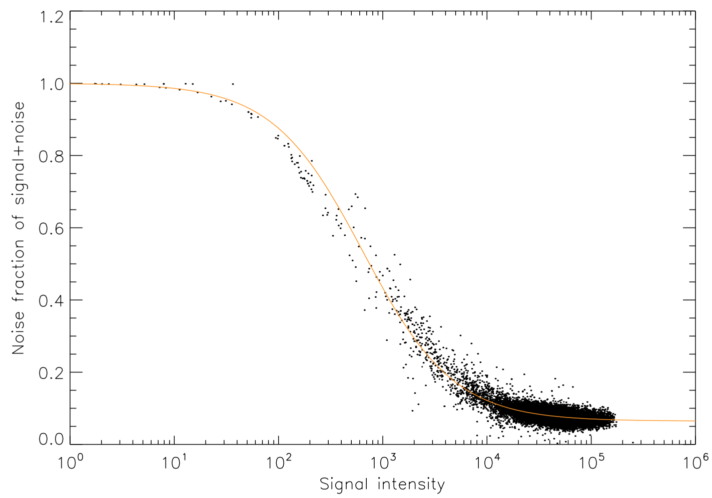

Figure 1: Noise fraction of total signal (signal + noise). Estimated from the total ASAR WM data-set May 2004 (26,930 imagetts).The Red line is based on model parameters: $\alpha = 0.069$ and $\sigma^2_{\mathrm{ad}} = 7.5 \cdot 10^2$

Data where the Fourier-domain is mainipulated

The model for azimuth Fourier profile given in equation (2) is based on the *ideal* data where no mainipulation is done (representing the raw-data), whereas the ASAR WM-mode data (processed with the Range-Doppler processor) is manipulated (redused bandwidth in both range and azimuth direction and multiplied with a 0.75 hamming window function) has to be described width a modified equation (where the noise is colored):

$$\tilde{b}(f) \;=\; b(f)\, h^2(f) \tag{5}$$

where h is the function *manipulating* the Fourier domain. Integrating out the Fourier domain we get the following expression for the observed intensity:

$$\tilde{I}_* \;=\; \lambda\, I + \mu\, \sigma^2_{\mathrm{noise}} \tag{6}$$

where I and $\sigma^2_{\mathrm{noise}}$ are the ideal case values and

$$\lambda \;\equiv\; \int df\, \tilde{a}^2(f - f_{\mathrm{dc}})\, h^2(f)\,, \tag{7}$$

$$\mu \;\equiv\; \int df\, \tilde{h}^2(f)\,. \tag{8}$$

The values of λ and μ are for different processing cases, given in Table 1. We observe that the noise level is larger in the outer looks than for the center look. This is also illustratet in Figure 2 where the *ideal* noise level is 1/10 of the signal intensity.

	λ	μ
Original data:	1.000000	1.000000
BW redused:	0.910851	0.663901
RD-processor:	0.614476	0.394022
Center look:	0.400612	0.216639
Side looks:	0.400612	0.389087

Table 1: The λ and μ parameters for the intensity in the bandwidth redused data (range bandwidth = 0.833 of the sample frequency and aziumth bandwidth = 0.796 of the PRF). in the ASAR WM Range-Doppler processor (azimuth 0.75 hamming window) and for center and side looks of the ASAR WM look extraction.

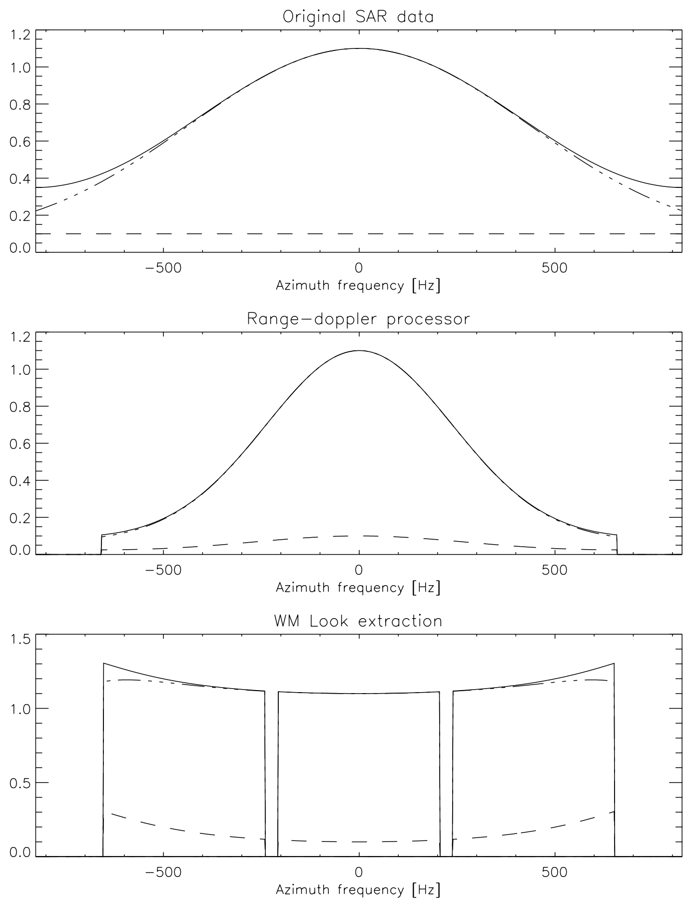

Figure 2: Azimuth profiles of SAR data, Upper plot is the original data, the center plot is processed by Range-doppler processor and the lower plot is the Wave-Mode look extxraction. The lines are: (dashed) Noise-level, (solid) Noise + aliazed signal, (dashed/dots) Noise + unaliazed signal.

What to do ?

I propose we use the fitted parameters in combination width the measured intensity $\tilde{I}_{\mathrm{rd}}$ of the range doppler imagettes to compute the realtive noise level for the different cases. By combining the equations we can write the *ideal* intensity as follows:

$$I = \frac{\tilde{I}_{\mathrm{rd}} - \mu_{\mathrm{rd}}\,\sigma_{\mathrm{ad}}^2}{\lambda_{\mathrm{rd}} + \mu_{\mathrm{rd}}\,\alpha} \tag{9}$$

and then find the relative noise-level for the different cases from:

$$\rho \;\equiv\; \frac{\mu\,\sigma_{\mathrm{noise}}}{\lambda\,I + \mu\,\sigma_{\mathrm{noise}}^2} \;=\; \frac{\mu\,(\sigma_{\mathrm{ad}}^2 + \alpha\,(I + \sigma_{\mathrm{ad}}^2))}{\lambda\,I + \mu\,(\sigma_{\mathrm{ad}}^2 + \alpha\,(I + \sigma_{\mathrm{ad}}^2))} \tag{10}$$

In this way, we only need to find the mean intensity of uncalibrated SLC image and use the fitted parameters α and σ_{ad}^2, and if we want to correct the code for additive noise, we simply multiply the given intensity with $(1-\rho)$ and only small changes to the code are needet.

Remark 1: the intensities are measured as the mean values of the uncalibratet images (abs(SLC)^2).

Remark 2: I am not sure this will work in the right direction (answere to Dr. Fab).